

IEEE TRANSACTIONS ON GEOSCIENCE AND REMOTE SENSING

A PUBLICATION OF THE IEEE GEOSCIENCE AND REMOTE SENSING SOCIETY



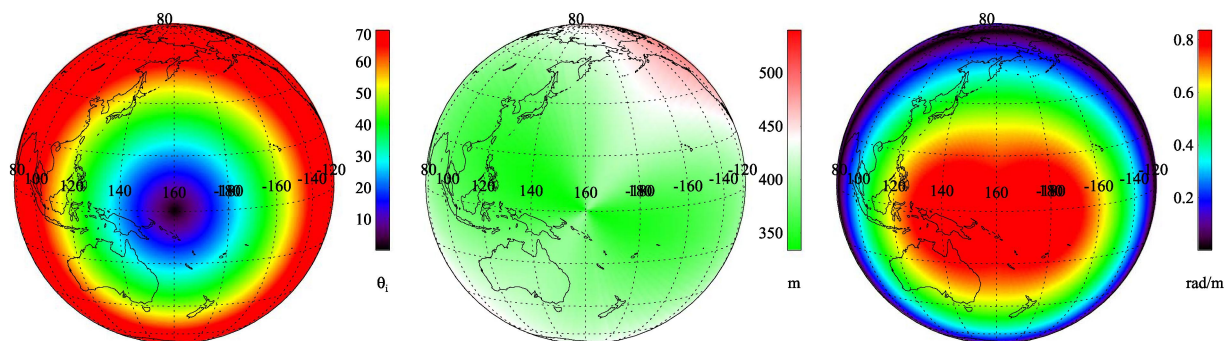
APRIL 2016

VOLUME 54

NUMBER 4

IGRSD2

(ISSN 0196-2892)



Incident angle, CoSAR azimuth resolution, and magnitude of range spectral shift after a 12-h observation period and a 300-s integration time.
(Left) Incident angle. (Middle) Cross-range (azimuth) resolution. (Right) Range spectral shift.

IEEE TRANSACTIONS ON GEOSCIENCE AND REMOTE SENSING

A PUBLICATION OF THE IEEE GEOSCIENCE AND REMOTE SENSING SOCIETY



APRIL 2016

VOLUME 54

NUMBER 4

IGRSD2

(ISSN 0196-2892)

REGULAR PAPERS

Atmosphere

- Effects of the Three-Dimensional Hydrometeor Distributions of Precipitating Clouds on Passive Microwave Rainfall Estimations *S.-W. Kim, D.-B. Shin, and Y. Choi* 1957
- Impact of Satellite Radiance Data on Simulations of Bay of Bengal Tropical Cyclones Using the WRF-3DVAR Modeling System *A. Routray, U. C. Mohanty, K. K. Osuri, S. C. Kar, and D. Niyogi* 2285

Oceans

- A Practical Method for On-Orbit Estimation of Polarization Response of Satellite Ocean Color Sensor. *X. He, D. Pan, Y. Bai, Z. Mao, T. Wang, and Z. Hao* 1967
- Oceanic Rain Flagging Using Radar Backscatter and Noise Measurements From Oceansat-2 Scatterometer. *B. S. Gohil, R. Sikhakolli, R. K. Gangwar, and A. S. Kiran Kumar* 2050
- Bayesian Estimation of Smooth Altimetric Parameters: Application to Conventional and Delay/Doppler Altimetry. *A. Halimi, C. Mailhes, J.-Y. Tournet, and H. Snoussi* 2207
- Water Depth Inversion From a Single SPOT-5 Dataset. *A. Poupardin, D. Idier, M. de Michele, and D. Raucoules* 2329

Vegetation and Land

- A Field Verification of an Algorithm for Retrieving Vegetation Water Content From Passive Microwave Observations *Y. Sawada, H. Tsutsui, T. Koike, M. Rasmy, R. Seto, and H. Fujii* 2082

Subsurface and Geology

- Adaptive Variable Time Fractional Anisotropic Diffusion Filtering for Seismic Data Noise Attenuation *Q. Zhou, J. Gao, Z. Wang, and K. Li* 1905

Electromagnetics

- A New Model for Sand-Ripple Scattering Based on SSA Method and Practical Ripple Profiles *P.-B. Wei, M. Zhang, W.-Q. Jiang, and D. Nie* 2450

Hyperspectral Data Processing

- Retrieval of the Ocean Skin Temperature Profiles From Measurements of Infrared Hyperspectral Radiometers—Part I: Derivation of an Algorithm. *E. W. Wong and P. J. Minnett* 1879

(Contents Continued on Page 1878)

Retrieval of the Ocean Skin Temperature Profiles From Measurements of Infrared Hyperspectral Radiometers—Part II: Field Data Analysis	<i>E. W. Wong and P. J. Minnett</i>	1891
Active-Metric Learning for Classification of Remotely Sensed Hyperspectral Images	<i>E. Pasolli, H. L. Yang, and M. M. Crawford</i>	1925
Anomaly Detection in Hyperspectral Images Based on Low-Rank and Sparse Representation	<i>Y. Xu, Z. Wu, J. Li, A. Plaza, and Z. Wei</i>	1990
ULGS II: A High-Performance Field and Laboratory Spectrogoniometer for Measuring Hyperspectral Bidirectional Reflectance Characteristics.	<i>C. A. Coburn and S. D. Noble</i>	2304
Probabilistic-Kernel Collaborative Representation for Spatial–Spectral Hyperspectral Image Classification	<i>J. Liu, Z. Wu, J. Li, A. Plaza, and Y. Yuan</i>	2371
Image Processing and Analysis		
Histogram-Based Attribute Profiles for Classification of Very High Resolution Remote Sensing Images	<i>B. Demir and L. Bruzzone</i>	2096
Dirichlet-Derived Multiple Topic Scene Classification Model for High Spatial Resolution Remote Sensing Imagery	<i>B. Zhao, Y. Zhong, G.-S. Xia, and L. Zhang</i>	2108
A Compressed-Sensing-Based Pan-Sharpener Method for Spectral Distortion Reduction	<i>M. Ghahremani and H. Ghassemian</i>	2194
Spatial-Hessian-Feature-Guided Variational Model for Pan-Sharpener	<i>P. Liu, L. Xiao, J. Zhang, and B. Naz</i>	2235
Enhanced Subpixel Mapping With Spatial Distribution Patterns of Geographical Objects	<i>Y. Ge, Y. Chen, A. Stein, S. Li, and J. Hu</i>	2356
Microwave Radiometry		
Differences Between the HUT Snow Emission Model and MEMLS and Their Effects on Brightness Temperature Simulation	<i>J. Pan, M. Durand, M. Sandells, J. Lemmetyinen, E. J. Kim, J. Pulliainen, A. Kontu, and C. Derksen</i>	2001
Faraday Rotation Correction for the SMAP Radiometer.	<i>D. M. Le Vine, S. Abraham, and J. Peng</i>	2070
Nodal Sampling: A New Image Reconstruction Algorithm for SMOS	<i>V. Gonzalez-Gambau, A. Turiel, E. Olmedo, J. Martinez, I. Corbella, and A. Camps</i>	2314
Band-Limited Signal Reconstruction From Irregular Samples With Variable Apertures	<i>D. G. Long and R. O. W. Franz</i>	2424
Radar Systems		
Multichannel Analysis and Suppression of Sea Clutter for Airborne Microwave Radar Systems	<i>V. Gracheva and J. Ender</i>	2385
Optimum Surface Roughness to Parameterize Advanced Integral Equation Model for Soil Moisture Retrieval in Prairie Area Using Radarsat-2 Data	<i>X. Bai, B. He, and X. Li</i>	2437
Synthetic Aperture Radar		
A Fast SAR Imaging Method for Ground Moving Target Using a Second-Order WVD Transform	<i>P. Huang, G. Liao, Z. Yang, X.-G. Xia, J.-T. Ma, and X. Zhang</i>	1940
A Synchronization Algorithm for Spaceborne/Stationary BiSAR Imaging Based on Contrast Optimization With Direct Signal From Radar Satellite.	<i>M. Zhang, R. Wang, Y. Deng, L. Wu, Z. Zhang, H. Zhang, N. Li, Y. Liu, and X. Luo</i>	1977
Change Detection Between SAR Images Using a Pointwise Approach and Graph Theory	<i>M.-T. Pham, G. Mercier, and J. Michel</i>	2020
Soil Moisture Estimation Using Hybrid Polarimetric SAR Data of RISAT-1	<i>G. G. Ponnurangam, T. Jagdhuber, I. Hajnsek, and Y. S. Rao</i>	2033
Robust Detection of Single and Double Persistent Scatterers in Urban Built Environments	<i>P. Ma and H. Lin</i>	2124
Unsupervised Learning of Generalized Gamma Mixture Model With Application in Statistical Modeling of High-Resolution SAR Images	<i>H.-C. Li, V. A. Krylov, P.-Z. Fan, J. Zerubia, and W. J. Emery</i>	2153
Interferometric Processing of Sentinel-1 TOPS Data	<i>N. Yague-Martinez, P. Prats-Iraola, F. Rodriguez Gonzalez, R. Brcic, R. Shau, D. Geudtner, M. Eineder, and R. Bamler</i>	2220
SAR Ground Moving Target Imaging Algorithm Based on Parametric and Dynamic Sparse Bayesian Learning.	<i>L. Yang, L. Zhao, G. Bi, and L. Zhang</i>	2254
Correlating Synthetic Aperture Radar (CoSAR)	<i>P. López-Dekker, M. Rodriguez-Cassola, F. De Zan, G. Krieger, and A. Moreira</i>	2268
Doppler Velocity Characteristics During Tropical Cyclones Observed Using ScanSAR Raw Data	<i>K. Kang, D. Kim, S. H. Kim, and W. M. Moon</i>	2343
CRIM-FCHO: SAR Image Two-Stage Segmentation With Multifeature Ensemble.	<i>H. Yu, L. Jiao, and F. Liu</i>	2400

A New Maximum-Likelihood Change Estimator for Two-Pass SAR Coherent Change Detection	2460
. <i>D. E. Wahl, D. A. Yocky, C. V. Jakowatz, Jr., and K. M. Simonson</i>	
Polarimetric Two-Scale Two-Component Model for the Retrieval of Soil Moisture Under Moderate Vegetation via L-Band SAR Data.	2470
. <i>G. Di Martino, A. Iodice, A. Natale, and D. Riccio</i>	
Global Navigation Satellite System	
Stochastic Modeling and Simulation of Delay–Doppler Maps in GNSS-R Over the Ocean	2056
. <i>G. Giangregorio, M. di Bisceglie, P. Addabbo, T. Beltramonte, S. D’Addio, and C. Galdi</i>	
Lidar Systems	
Robust Locally Weighted Regression Techniques for Ground Surface Points Filtering in Mobile Laser Scanning Three Dimensional Point Cloud Data.	2181
. <i>A. Nurunnabi, G. West, and D. Belton</i>	
Satellite Systems	
Corrections for On-Orbit ATMS Lunar Contamination.	1918
. <i>H. Yang and F. Weng</i>	
Improvement of the PARASOL Radiometric In-Flight Calibration Based on Synergy Between Various Methods Using Natural Targets	2140
. <i>B. Fougnie</i>	
Developing Daily Cloud-Free Snow Composite Products From MODIS Terra–Aqua and IMS for the Tibetan Plateau	2171
. <i>J. Yu, G. Zhang, T. Yao, H. Xie, H. Zhang, C. Ke, and R. Yao</i>	

About the Cover: The cover figure shows the incident angle, achieved azimuth resolution and range spectral shift for an exemplary geosynchronous Correlating Synthetic Aperture Radar (CoSAR) mission concept. A CoSAR system allows imaging of the second-order statistics of fast decorrelating distributed targets, in particular the ocean surfaces. This is achieved by combining the radar echoes received simultaneously by two radar systems with a relative motion in the *azimuth* direction. In this particular example, the two quasi-geostationary radar satellites are on the opposite sides of an approximately circular trajectory, allowing imaging twice per day a large, incident-angle limited region. The intended products of such a mission would include the Normalized Radar Cross Section, a cross-track interferometric phase, and the Doppler frequency, allowing the retrieval of surface winds, mean surface height, and surface currents. For more information please see “Correlating Synthetic Aperture Radar (CoSAR),” by López-Dekker *et al.*, which begins on page 2268.